Mon. Not. R. Astron. Soc. **349,** 1481–1492 (2004) doi:10.1111/j.1365-2966.2004.07623.x

UBVRI CCD photometric study of the open clusters Basel 4 and NGC 7067

R. K. S. Yadav[1]★ and Ram Sagar[2]★

[1] *Inter-University Centre for Astronomy and Astrophysics, Ganeshkhind, Pune 411 007, India*
[2] *State Observatory, Manora Peak, Nainital 263 129, India*

Accepted 2004 January 12. Received 2004 January 12; in original form 2003 July 4

ABSTRACT

In this paper we present *UBVRI* CCD photometry in the region of two young open star clusters Basel 4 and NGC 7067 for the first time. Our sample consists of ∼4000 stars down to $V \sim 21$ mag. Stellar surface density profile indicates that radii of Basel 4 and NGC 7067 are about 1.8 and 3.0 arcmin respectively. The $(U - B)$ versus $(B - V)$ diagrams indicate that the metallicity of NGC 7067 is solar while that of Basel 4 is $Z \sim 0.008$. We estimate the mean value of $E(B - V) = 0.45 \pm 0.05$ and 0.75 ± 0.05 mag for Basel 4 and NGC 7067, respectively. The analysis of 2MASS *JHK* data in combination with the optical data in both the clusters yields $E(J - K) = 0.30 \pm 0.20$ mag and $E(V - K) = 1.60 \pm 0.20$ mag for Basel 4 while $E(J - K) = 0.40 \pm 0.20$ mag and $E(V - K) = 2.10 \pm 0.20$ mag for NGC 7067. Furthermore, colour excess diagrams show a normal interstellar extinction law towards both the clusters.

Using the intrinsic colour–magnitude diagrams of the cluster members, we estimated the distances of the clusters as 3.0 ± 0.2 and 3.6 ± 0.2 kpc for Basel 4 and NGC 7067, respectively. By fitting the proper metallicity isochrones to the bright cluster members we estimated the age of the clusters as 200 ± 50 and 100 ± 25 Myr for Basel 4 and NGC 7067, respectively. The mass function slopes that are derived by applying the corrections of field star contamination and data incompleteness are 1.55 ± 0.25 and 1.68 ± 0.47 for Basel 4 and NGC 7067, respectively. The values of the mass function slope are thus not very different from Salpeter's value. Mass segregation is observed in both the clusters, which may be caused by the dynamical evolution or the imprint of star formation processes or both.

Key words: Hertzsprung–Russell (HR) diagram – stars: luminosity function, mass function – dust, extinction – open clusters and associations: individual: Basel 4 – open clusters and associations: individual: NGC 7067.

1 INTRODUCTION

Open clusters are ideal objects for the study of the Galactic disc. The young open clusters are used to determine spiral arm structure, to investigate the mechanisms of star formation and its recent history, and to constrain the initial luminosity and mass function in aggregates of stars etc. For such studies, it is important to know the basic parameters of the clusters. The colour–magnitude (CM) and colour–colour (CC) diagrams of an open cluster are valuable tools for obtaining basic information, such as cluster distance and age, and for studying interstellar extinction in the directions of both cluster and stellar evolution. An important aspect for understanding star formation and stellar evolution is the following question: how many stars, of which masses, formed or exist in an ensemble of stars? A function that describes the frequency distribution of stellar masses is called the stellar mass function. Star clusters are suitable objects for mass function determination as members formed (more or less) at the same time and from the same cloud. In addition to this, study of mass segregation in open clusters provides a clue about the spatial distribution of high- and low-mass stars within the clusters. Generally, it is found that high-mass stars are concentrated towards the centre of the clusters in comparison to lower mass stars. The cause of such kinds of distribution is still not well understood, but might relate to either dynamical evolution or the imprint of star formation itself.

In the light of above discussions, we conducted *UBVRI* CCD stellar photometry in two young open star clusters Basel 4 and NGC 7067, aiming to investigate the cluster's basic parameters (e.g. reddening, distance and age), mass function and mass segregation etc. The existing basic information on both the clusters is given in Table 1. The plan of the paper is as follows. In Section 2 we summarize the previous studies of Basel 4 and NGC 7067, while Section 3 is dedicated on the observation and data reduction strategies. Section 4 deals with the determination of clusters basic parameters as well as detail study of interstellar extinction, mass function and mass segregation in the clusters under study. Finally, Section 5 summarizes our findings.

★E-mail: rkant@iucaa.ernet.in (RKSY); sagar@upso.ernet.in (RS)

Table 1. General information about the clusters under study taken from Dias et al. (2002).

Cluster	IAU	OCL	l (deg)	b (deg)	Trumpler class	Radius (arcmin)	Distance (kpc)	$E(B-V)$ (mag)	log(age) (yrs)
Basel 4	C0545+302	455	179.23	1.20	II 1p	2.5	5.6	0.53	7.0
NGC 7067	C2122+478	208	91.19	−1.67	II 1p	1.5	1.3	0.85	7.5

2 EARLIER INVESTIGATIONS

Basel 4. This cluster was first studied by Svolopoulos (1965) photographically in the RGU system. According to him the location of this cluster coincides with spiral arm +III, which could be expected – if it exists at all – to be at a similar distance. In any case, it is remarkable that typical representatives of the Galactic disc population are located so far out in the direction of the Galactic anticentre. He classified this cluster as a III 2m. In addition to this, he also concluded that Basel 4 is 2×10^7 yr old, and has a total apparent diameter of 6.4 arcmin at a distance of 5.9 kpc. To our knowledge no other studies have been carried out so far.

NGC 7067. This cluster was first studied by Becker (1963). It is a poor young open cluster lying in the Cygnus spiral arm. It was again revisited by Becker (1965) and indicated that the earliest spectral type of the cluster member is b0.5. He also estimated the cluster angular diameter of 2.1 arcmin, which corresponds to a linear diameter of 2.6 pc. Hassan (1973) also studied this cluster photoelectrically and derived a distance of about 4.4 kpc, with $E(B-V) = 0.83$ Mag and age less than 10^7 yr. Dias et al. (2002) mentioned a distance of 1.3 kpc for this cluster. The distance determination to the cluster is thus quite uncertain.

3 OPTICAL OBSERVATIONS AND DATA REDUCTIONS

3.1 CCD photometric observations

We used CCD imaging to obtain *UBV* Johnson and *RI* Cousins photometry of the stars in the region of the open clusters Basel 4 and NGC 7067 on 2000 January 02/03 and 2001 Oct 11/12 respectively. The data were obtained using the 2K × 2K CCD system at the $f/13$ Cassegrain focus of the 104-cm Sampurnanand telescope of the State Observatory, Naini Tal. A log of the CCD observations is given in Table 2. The 0.36 arcsec pixel^{-1} plate scale resulted in a field of view of 12.3 × 12.3 arcmin^2. The readout noise and gain of the CCD are 5.3 e$^-$ and 10 e$^-$ ADU^{-1} respectively. For accurate photometric measurements of fainter stars, 2 to 3 deep exposures were taken in each passband. Furthermore, observations were taken in 2 × 2 pixel binning mode to improve the signal to noise ratio (S/N). An identification map of cluster and field regions for both the clusters is shown in Fig. 1. Besides these clusters, a number of standard star field were also observed for calibration purposes. We observed M67 (open cluster) and field PG0231+051 of Landolt (1992) for calibrating Basel 4 and NGC 7067 respectively. The V mag range of stars used for calibration is 11–13 mag in M67 and 12–16 mag in PG0231+051 while the $(V-I)$ colour range is 0.5–1.1 mag in M67 and −0.5–2.0 in PG0231+051. Thus, the standard stars in these fields provide a good magnitude and colour coverage, essential to obtain reliable photometric transformations. The standard field are also observed in *UBVRI* at different airmasses to obtain a reliable estimate of the atmospheric extinction coefficients. For correcting the bias level to the image, a number of bias frame were taken during the observations while for the flat-field correction a number of flat frames were taken on the twilight sky in each filter.

Table 2. Log of CCD observations along with equatorial coordinates for the epoch 2000.

Region	Filter	Exposure Time (in seconds)	Date
Basel 4	U	1800 × 2, 300 × 1	2000 Jan 02/03
$\alpha_{2000} = 07^h32^m00^s$	B	1200 × 2, 180 × 1	”
$\delta_{2000} = +30^d12'57''$	V	900 × 2, 120 × 1	”
	R	240 × 3, 60 × 1	”
	I	240 × 3, 60 × 1	”
NGC 7067	U	1800 × 3, 300 × 2	2001 Oct 11/12
$\alpha_{2000} = 21^h24^m11^s$	B	1200 × 3, 240 × 2	”
$\delta_{2000} = +48^d00'57''$	V	900 × 3, 180 × 2	”
	R	600 × 3, 120 × 2	”
	I	300 × 3, 60 × 2	”

3.2 Data reduction

The CCD images were processed using the IRAF data reduction package. Then, for a given filter, frames of the same exposure time were combined into one, to improve the statistics of the faintest stars. Instrumental magnitudes were derived through Point Spread Function (PSF) fitting using DAOPHOT (Stetson 1987) within MIDAS. During the process of determining the PSF, we used several well-isolated stars to construct a single PSF for the entire frame on each exposure. The bright stars were measured on the frames with short exposure times, as they were saturated in the longer exposure frames.

For transforming the instrumental magnitude to the standard magnitude, the photometric calibration equations are as follows:

$$u = U + 6.40 \pm 0.01 - (0.03 \pm 0.02)(U-B) + 0.59X,$$
$$b = B + 4.39 \pm 0.01 - (0.02 \pm 0.01)(B-V) + 0.36X,$$
$$v = V + 4.08 \pm 0.01 - (0.01 \pm 0.01)(B-V) + 0.23X,$$
$$r = R + 4.00 \pm 0.01 - (0.02 \pm 0.01)(V-R) + 0.18X,$$
$$i = I + 4.55 \pm 0.01 - (0.01 \pm 0.02)(R-I) + 0.13X,$$

where U, B, V, R and I are the standard magnitudes and u, b, v, r and i are the instrumental aperture magnitudes normalized for 1 s of exposure time and X is the airmass. We have ignored the second-order colour correction terms as they are generally small in comparison to other errors present in the photometric data reduction. The errors in zero-point and colour coefficients are estimated from the deviation of data points from the linear relation and are ∼0.01 mag. Using these transformation equation, we calibrated the CCD instrumental magnitudes. For generating the local standards, we selected many well-isolated stars in the observed region and used the DAOGROW programme for the construction of an aperture growth curve required for determining the difference between aperture and profile fitting magnitudes. Table 3 gives the photometric errors as a function of magnitude. The internal errors estimated in the S/N ratio of the stars as the output of ALLSTAR mainly produce scatter in the various CC and CM diagrams of the clusters. It can be seen that the errors become large (⩾0.1 mag) for stars fainter than $V =$ 20 mag, so the measurements should be considered unreliable below this magnitude. The final photometric data are available in electronic

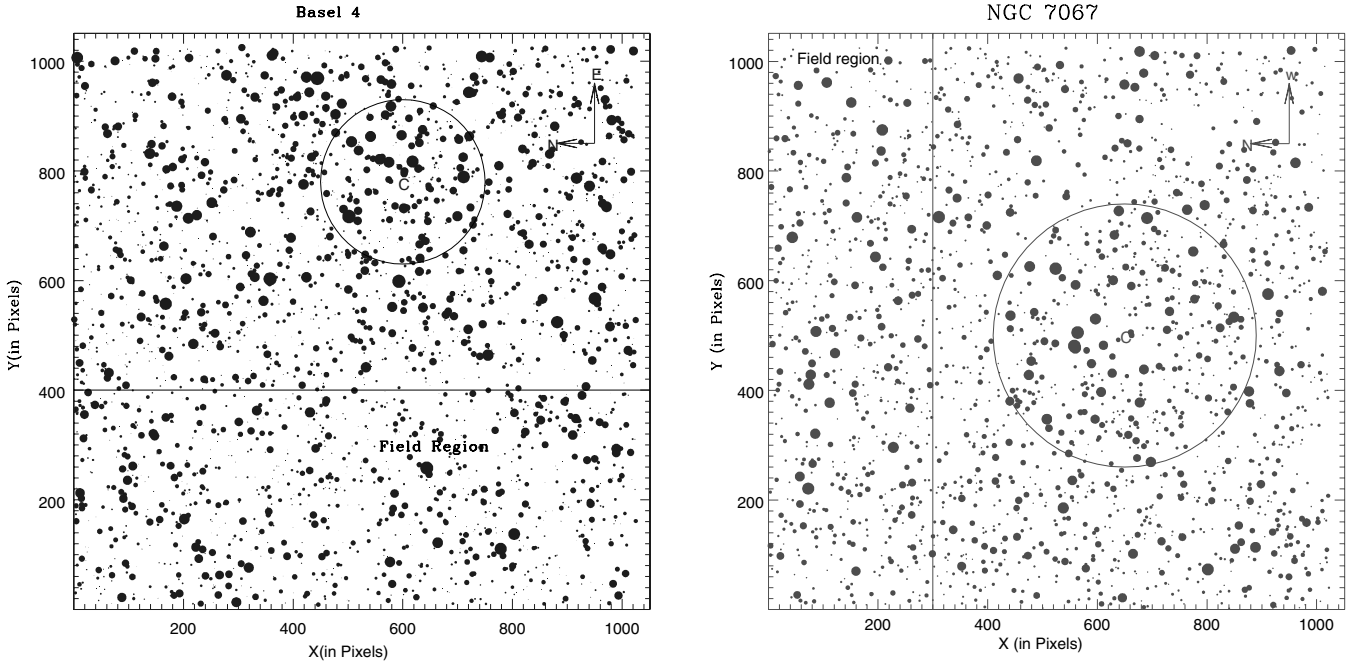

Figure 1. Identification maps for the cluster and field regions of Basel 4 and NGC 7067. The (X, Y) coordinates are in pixel units corresponding to 0.72 arcsec on the sky. Direction is indicated in the corresponding map. Filled circles of different sizes represent the brightness of the stars: the smallest size denotes stars of $V \sim$21 mag. Open circles having their centre at 'C' in the map represent the respective cluster size.

Table 3. Internal photometric errors in magnitude as a function of brightness. σ is the standard deviation per observation in magnitude.

Magnitude range	σ_U	σ_B	σ_V	σ_R	σ_I
$\leqslant$12.0	0.01	0.01	0.01	0.01	0.01
12.0–13.0	0.01	0.01	0.01	0.01	0.01
13.0–14.0	0.01	0.01	0.01	0.01	0.01
14.0–15.0	0.01	0.01	0.01	0.01	0.01
15.0–16.0	0.01	0.01	0.01	0.01	0.01
16.0–17.0	0.02	0.01	0.01	0.01	0.02
17.0–18.0	0.03	0.02	0.02	0.02	0.03
18.0–19.0	0.04	0.05	0.03	0.05	0.06
19.0–20.0	0.05	0.09	0.05	0.09	0.08

form at the WEBDA site [1] and also from the authors. The format of the table is listed in Table 4 for Basel 4 and NGC 7067.

3.3 Comparison with previous photometric study

As mentioned in Section 2, only NGC 7067 has photoelectric data given by Becker (1965), and we compared our data with these data. Table 5 presents average differences (in the sense of our values minus those of other origin) along with their standard deviations. The difference Δ in V, $(B-V)$ and $(U-B)$ are plotted in Fig. 2. Table 6 and Fig. 2 indicate that our V magnitudes are systematically brighter by $\sim$0.05 mag without any dependence on the stellar magnitude. The $\Delta(B-V)$ values show good agreement with the photoelectric data, while $\Delta(U-B)$ show a decreasing trend with the V mag.

[1] http://obswww.unige.ch/webda/

Table 4. CCD relative (X, Y) positions and V, $(U-B)$, $(B-V)$, $(V-R)$ and $(V-I)$ photometric magnitudes of few stars, as a sample measured in the region of the cluster Basel 4 and NGC 7067. Stars are numbered in increasing order of X value. The last column represent the photometric membership information where m and nm represent the member and non-member stars respectively.

Star	X (pixel)	Y (pixel)	V (mag)	$(U-B)$ (mag)	$(B-V)$ (mag)	$(V-R)$ (mag)	$(V-I)$ (mag)	Mem
				Basel 4				
1	1.87	701.86	19.64	*	*	0.69	1.61	nm
2	2.01	519.82	18.76	*	*	0.40	1.17	nm
3	2.71	790.32	20.66	*	*	0.48	1.52	nm
4	2.87	30.33	19.63	*	*	0.58	1.21	nm
5	3.34	877.65	20.33	*	*	0.33	1.34	nm
				NGC 7067				
1	1.69	835.80	19.37	*	*	0.68	1.61	nm
2	3.47	214.41	19.57	*	*	0.83	1.93	nm
3	3.87	116.54	17.60	*	*	1.24	2.91	nm
4	3.94	99.46	19.33	*	*	0.88	1.87	nm
5	4.01	496.79	20.22	*	*	0.78	1.70	nm

3.4 Near-IR data

We have used the Two Micron All Sky Survey (2MASS) J(1.25 μm), H(1.65 μm) and K_s (2.17 μm) data for both clusters Basel 4 and NGC 7067. 2MASS data are taken from observations with two highly automated 1.3-m telescopes: one at Mount Hopkins, AZ, and the other at Cerro Tolalo Inter-American Observatory (CTIO), Chile. The data are complete up to 16.0 mag in J, 15.5 mag in H and 15.0 in K_s. The uncertainty is 0.155 mag for a star of $K_s \sim$ 16.5 mag. The K_s magnitudes are converted into K magnitude following Persson et al. (1998). 2MASS data are available at the web site http://www.ipac.caltech.edu/2MASS/.

Table 5. Comparison of our photometry with Becker (1965) for the cluster NGC 7067. The difference (Δ) is always in the sense present minus comparison data. The mean and standard deviations in magnitude are based on N stars. A few deviated points are not included in the average determination.

Cluster	Comparison data	V range	$\langle\Delta V\rangle$ Mean$\pm\sigma$(N)	$\langle\Delta(B-V)\rangle$ Mean$\pm\sigma$(N)	$\langle\Delta(U-B)\rangle$ Mean$\pm\sigma$(N)
NGC 7067	Becker (1965)	<14.0	$0.06 \pm 0.03(4)$	$-0.10 \pm 0.03(4)$	$0.07 \pm 0.14(4)$
		14.0–15.0	$0.06 \pm 0.04(11)$	$-0.02 \pm 0.02(10)$	$-0.07 \pm 0.08(10)$
		15.0–16.0	$-0.07 \pm 0.09(14)$	$-0.006 \pm 0.04(10)$	$0.06 \pm 0.12(9)$

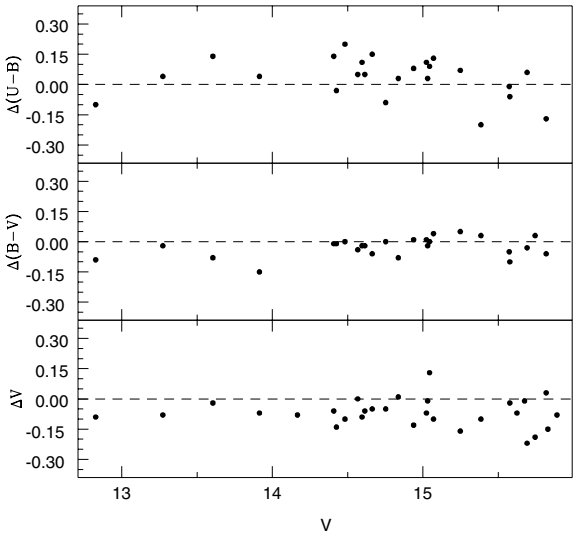

Figure 2. Comparison of our photometry with photoelectric data of Becker (1965) for NGC 7067.

Table 6. Frequency distribution of the stars in the $V, (V-I)$ diagram of the cluster and field regions. N_B, N_S and N_R denote the number of stars in a magnitude bin blueward, along and redward of the cluster sequence respectively. The number of stars in the field regions are corrected for area differences. N_C (difference between the N_S value of cluster and field regions) denotes the statistically expected number of cluster members in the magnitude bin.

	Basel 4							NGC 7067						
V range	Cluster region			Field region				Cluster region			Field region			
	N_B	N_S	N_R	N_B	N_S	N_R	N_C	N_B	N_S	N_R	N_B	N_S	N_R	N_C
12–13	0	2	0	0	0	0	2	0	1	2	0	0	0	1
13–14	0	2	0	0	0	0	2	0	2	3	1	1	4	1
14–15	0	4	3	0	0	1	4	0	4	11	0	0	6	4
15–16	0	8	5	0	2	3	6	0	3	8	0	1	4	2
16–17	0	11	4	1	5	3	6	0	12	8	0	4	16	8
17–18	0	16	8	4	7	4	9	0	17	11	1	7	19	10
18–19	2	17	5	7	9	2	8	5	35	20	2	17	36	18
19–20	3	22	3	9	9	1	13	18	44	19	10	23	61	21

4 ANALYSIS OF THE DATA

4.1 Cluster radius and radial stellar surface density

For a reliable determination of cluster parameters it is essential to know about the radial extent of the cluster. According to Mermilliod (1995), Basel 4 and NGC 7067 has a diameter of 5 and 3 arcmin, so our study covers the entire cluster region. To estimate the cluster radius, we derive the surface stellar density by performing star counts in concentric rings around the estimated centre of the cluster, and then dividing by their respective areas. The centre of the cluster is determined iteratively by calculating the average X and Y positions of the stars within 300 pixels from an eye-estimated centre, until they converged to a constant value. The pixel coordinates of the cluster centre obtained in this way are (600, 780) and (690, 700) for Basel 4 and NGC 7067 respectively. There may be a few tens of pixels error in locating the cluster centre. Centre of the clusters are marked by 'C' in the identification maps (Fig. 1). The radial density profile and the corresponding Poisson error bars are depicted in Fig. 3. A clear radius density gradient present in Basel 4 confirms the existence of

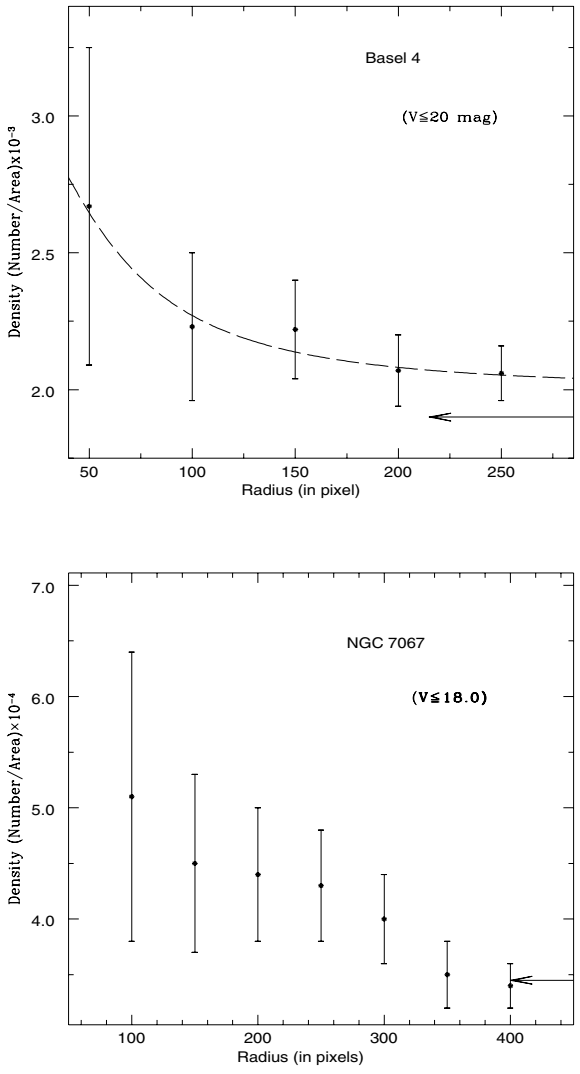

Figure 3. Radial density profile for Basel 4 and NGC 7067. The length of the error bar denotes errors resulting from sampling statistics ($= \frac{1}{\sqrt{N}}$ where N is the number of stars used in the density estimation at that point). Dotted curves represent the fitted profile and arrows represent the level of field star densities.

clustering. In NGC 7067 the density profile decreases with radius slowly up to the limit of the covered region. Following Kaluzny (1992), we describe the $\rho(r)$ of an open cluster as

$$\rho(r) \propto \frac{f_0}{1+(r/r_c)^2},$$

where the cluster core radius r_c is the radial distance at which the value of $\rho(r)$ becomes half of the central density f_0. We fit this function to the observed data points in the cluster Basel 4 and use χ^2 minimization technique to determine r_c and other constants. As can be seen in Fig. 3, the fitting of the function is satisfactory for Basel 4. Such fitting could not be done in NGC 7067 owing to large errors in the values of $\rho(r)$. In the cluster Basel 4, values of $\rho(r)$ flatten at larger radii, indicating the level of probable field star density in the cluster direction shown by arrow in Fig. 3. The field star density thus obtained is 2.1×10^{-3} pixel^{-2} for Basel 4. In the case of NGC 7067, the field star density has been estimated as 0.3×10^{-3} pixel^{-2} based on the last two data points of its radial density profile in Fig. 3. The radius at which the value of ρ becomes approximately equal to the field star density has been considered as the cluster radius. The values determined in this way are 1.8 and 3.0 arcmin for Basel 4 and NGC 7067 respectively. Present radius estimates are lower, with the value listed in Table 1 for Basel 4 while in the case of NGC 7067 our estimated value is larger (see Table 1).

As the observed area is much larger than the cluster area, we have considered stars having more than 2.5 and 1.6 cluster radius as field stars for the cluster Basel 4 and NGC 7067 respectively (see Fig. 1). The areas of the field regions are 4.2×10^5 and 3.1×10^5 pixel^2 for the cluster Basel 4 and NGC 7067 respectively. For Basel 4, the closest boundary of the field region is about 4.5 arcmin away from the cluster centre in the west direction while for NGC 7067, it is about 5.0 arcmin away in the north direction. For the further analysis we have considered the stars laying within cluster radius.

4.2 Apparent CM diagrams of the cluster regions

The apparent CM diagrams of Basel 4 and NGC 7067 for the stars present within the cluster radius are shown in Fig. 4. The detection in the *U* filter is not as deep as in *BVRI* because of the low quantum efficiency of the CCD detector in *U* region. So, there are large number of stars without any *U* measurements. A well-defined cluster MS contaminated by field stars is clearly visible in the CM diagrams of Basel 4 while in NGC 7067 the MS is not so well populated because of the poorness of the cluster. In the cluster NGC 7067, the stars on the red side of the MS appear to form a sequence parallel to the MS and that can be ascribed owing to Galactic disc field stars. The field star contamination increases with decreasing brightness. The cluster sequence fainter than $V \sim 16$ mag in Basel 4 and $V \sim 18$ mag in NGC 7067 have larger scatter. This may be caused by photometric errors as well as field star contamination. It is difficult to separate field stars from the cluster members. For the separation of cluster members from the field stars, precise proper motion and/or radial velocity measurements of these stars are required. In the absence of such data for these clusters, we selected members by defining the binary sequence. It has been defined by shifting the blue envelope by 0.8 mag vertically, which is shown in the CM diagrams of the clusters. Some stars, in spite of their ambiguous positions, could not definitively be rejected as likely cluster members. From the V, $(V-I)$ diagram of the field region, the statistically expected number of field stars among the photometric cluster members has been given in Table 6. The frequency distribution of the field star contamination in different part of the CM diagram can be estimated from the Table 6. It is thus clear that all photometric probable members cannot be cluster members and non-members should be subtracted in the studies of cluster MF etc. However, probable members located within a cluster radius from its centre can be used to determine the cluster parameters, as they have relatively less field star contamination and this has been done in the sections to follow.

4.3 Interstellar extinction towards the clusters

Fig. 5 shows the $(U-B)$ versus $(B-V)$ diagrams for determining the interstellar extinction using the probable cluster members. We fit the intrinsic zero-age main-sequence (ZAMS) given by Schmidt-Kaler (1982) valid for stars of luminosity class V to the MS stars of spectral type earlier than A0 assuming the slope of reddening $E(U-B)/E(B-V)$ as 0.72.

In the cluster Basel 4, the ZAMS given by Schmidt-Kaler (1982) does not fit well for the stars of spectral type A, F and G. Excess in $(U-B)$ colour is clearly visible for the stars of $(B-V) > 0.50$ mag. This indicates that the cluster is metal-deficient. The UV excess $\delta(U-B)$ determined with respect to Hyades MS turns out to be $\sim$0.1 mag. Using the [Fe/H] versus $\delta(U-B)$ relation of Carney (1979) we estimated [Fe/H] ~ -0.35 which correspond to $Z \sim 0.008$. To estimating the reddening in the direction of this cluster we therefore fitted the ZAMS given by Schaerer et al. (1993) for $Z = 0.008$ which is shown by short-dashed lines in the two-colour diagram of Basel 4. The ZAMS of $Z = 0.008$ fits nicely and provides the reddening $E(B-V) = 0.45 \pm 0.05$ for this cluster, which is in agreement with the earlier findings (see Table 1).

Unlike Basel 4, in the cluster NGC 7067, ZAMS given by Schmidt-Kaler (1982) for the solar metallicity fits both early- and late-type stars. The fitted values of $E(B-V)$ vary from 0.70 to 0.80 mag. The mean value is $E(B-V) = 0.75 \pm 0.05$ mag. Our mean reddening estimate for the imaged region agree fairly well with values estimated earlier by others (see Table 1).

We investigate the nature of interstellar extinction law towards the clusters, by considering the stars having spectral type earlier than A0. This has been selected from their position in the $(U-B)$ versus $(B-V)$ and apparent CM diagrams which reveals that bright stars with $V < 16.0$ mag and $(B-V) < 0.60$ mag in Basel 4 and with $V < 16.5$ mag and $(B-V) < 0.75$ mag in NGC 7067 are required stars. The number of such stars are 11 and 12 in Basel 4 and NGC 7067 respectively. The intrinsic colours for these stars have been determined using *UBV* photometric *Q* method (cf. Johnson & Morgan 1953; Sagar & Joshi 1979) and the calibrations given by Caldwell et al. (1993) for $(U-B)_0$, $(V-R)_0$ and $(V-I)_0$ with $(B-V)_0$. The mean values of the colour excess ratios derived in this way are listed in Table 7 for both the clusters. They indicate that the law of interstellar extinction in the direction of the clusters under discussion is normal.

4.3.1 Interstellar extinction in near-IR

By using the optical and infrared data, we estimated the interstellar extinction for both clusters under study. There are 65 and 44 common stars in the cluster Basel 4 and NGC 7067 within the cluster radius respectively. Fig. 6 shows the $(J-K)$ versus $(V-K)$ diagrams and fit a ZAMS for metallicity $Z = 0.008$ taken from Schaerer et al. (1993) in the cluster Basel 4 and $Z = 0.02$ taken from Schaller et al. (1992) in the cluster NGC 7067. This gives $E(J-K) = 0.30 \pm 0.20$ mag and $E(V-K) = 1.60 \pm 0.20$ mag for the cluster Basel 4 and $E(J-K) = 0.40 \pm 0.20$ mag and $E(V-K) = 2.10 \pm 0.20$ mag

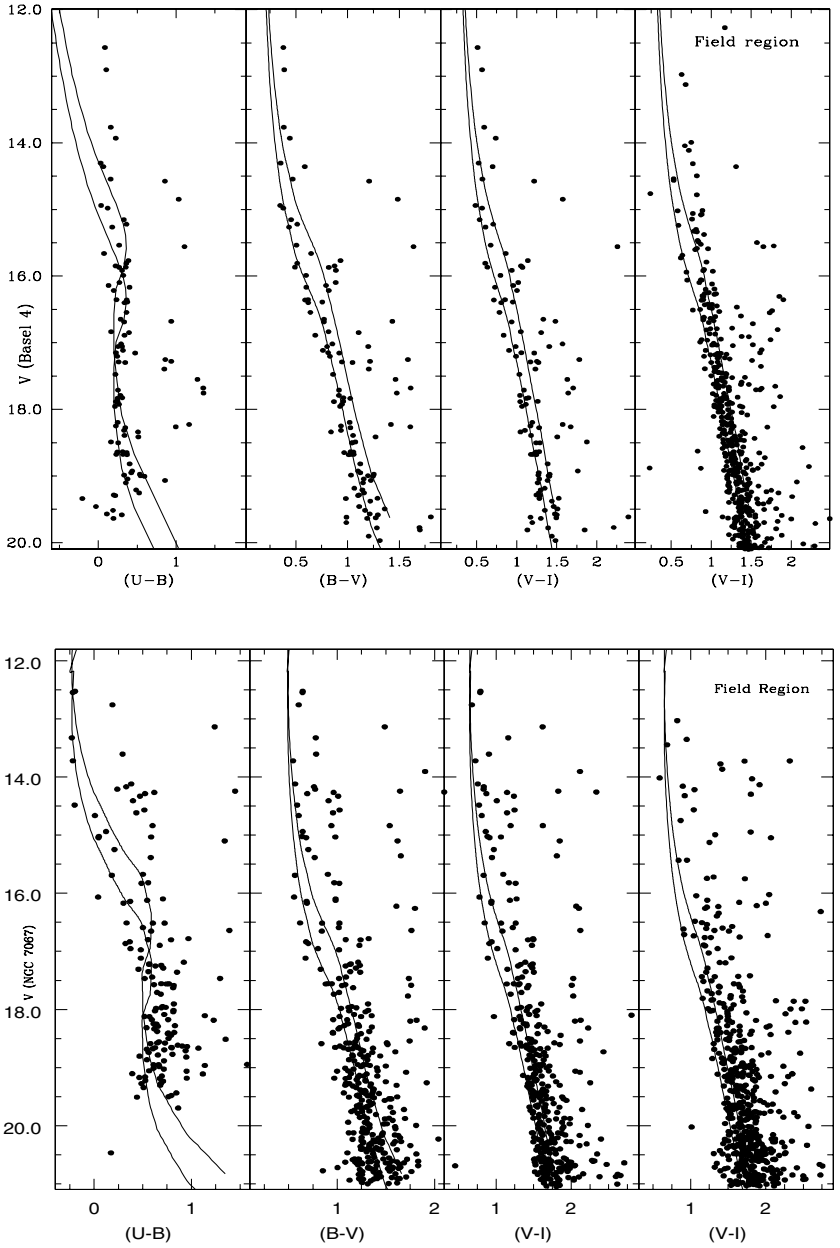

Figure 4. The V, $(U-B)$; V, $(B-V)$ and V, $(V-I)$ diagrams for the stars observed by us in the Basel 4 and NGC 7067 cluster regions and V, $(V-I)$ CM diagrams of the corresponding field regions. Solid lines represent the blue and red envelope of the cluster MS. The red envelope is determined by shifting the blue envelope vertically by 0.80 mag.

for the cluster NGC 7067. For both clusters the ratio $\frac{E(J-K)}{E(V-K)} \sim 0.20 \pm 0.30$ is in good agreement with the normal interstellar extinction value 0.19 suggested by Cardelli et al. (1989). However, scattering is larger owing to the error size in *JHK* data.

4.3.2 The law of interstellar extinction

We used the colour excess ratio method described by Johnson (1968) for the study of interstellar extinction law in the direction of both clusters under study. For this we used the stars of spectral type earlier than A0. We determined the colour excesses by comparing the observed colours of the stars with its intrinsic colours derived from the MKK spectral type–luminosity class colour relation given by FitzGerald (1970) for $(U-V)$ and $(B-V)$; by Johnson (1966) for $(V-R)$ and $(V-I)$; and by Koornneef (1983) for $(V-J)$, $(V-H)$ and $(V-K)$. For normalization, we selected the $E(V-J)$ colour excess for reasons described in Yadav & Sagar (2002). In Fig. 7 we plot the colour excess $E(U-B)$, $E(B-V)$, $E(V-R)$, $E(V-I)$, $E(V-H)$ and $E(V-K)$ against $E(V-J)$. In this figure, the straight line represents the least-squares linear fit to the data points. The values of correlation coefficient (r) and fit indicate that the data points are well represented by linear relation. The slopes of these straight lines as given in Table 8 represent reddening directions in the form of colour excess ratios. For comparison, the colour excess ratios given by Cardelli et al. (1989) for the normal interstellar matter are also listed in Table 8. The present reddening directions agree well with those.

In addition to this we have also estimated the value of R, in order to know more about the nature of the interstellar extinction law in

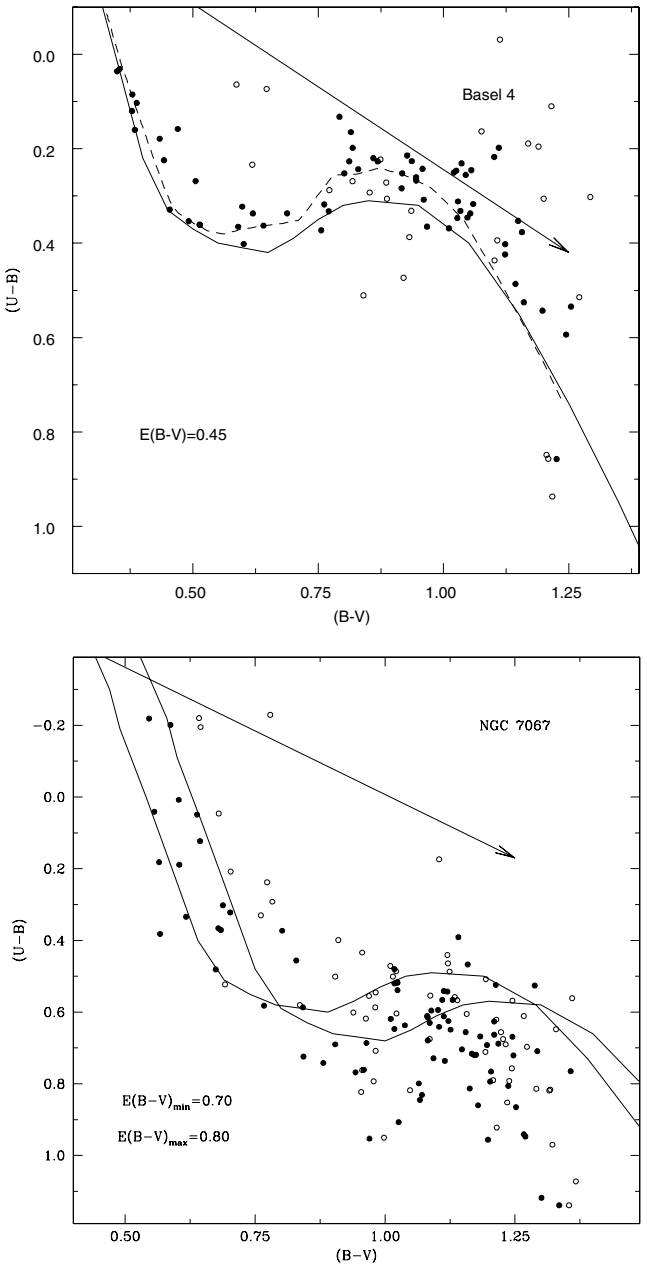

Figure 5. The $(U - B)$ versus $(B - V)$ diagrams of the stars in the cluster region for Basel 4 and NGC 7067. Stars considered as non-members in Fig. 4 are shown as open circles. The arrow represents slope 0.72 and the direction of the reddening vector. The solid curve represents the locus of Schmidt-Kaler's (1982) ZAMS fitted for the marked values of colour excesses. The curve shown by short-dashed lines in Bessel 4 is the ZAMS given by Schaerer et al. (1993) for $Z = 0.008$.

the direction of the clusters under study. We used the relation $R = 1.1E(V - K)/E(B - V)$ (Whittet & van Breda 1980), which is generally used at longer wavelengths. The average values of $R = 3.51 \pm 0.30$ (sd) and 3.04 ± 0.22 (sd) for Basel 4 and NGC 7067 respectively are not too different from the value 3.1 for a normal extinction law.

In the light of the above analysis, we conclude that the interstellar extinction law is normal towards both Basel 4 and NGC 7067, in agreement with our earlier result.

Table 7. A comparison of the colour excess ratios with $E(B - V)$ for both star clusters with the corresponding values for the normal interstellar extinction law given by Cardelli, Clayton & Mathis (1989).

Objects	$\frac{E(U-B)}{E(B-V)}$	$\frac{E(V-R)}{E(B-V)}$	$\frac{E(V-I)}{E(B-V)}$
Normal interstellar	0.72	0.65	1.25
Basel 4	0.71 ± 0.05	0.68 ± 0.04	1.33 ± 0.10
NGC 7067	0.69 ± 0.04	0.56 ± 0.02	1.33 ± 0.08

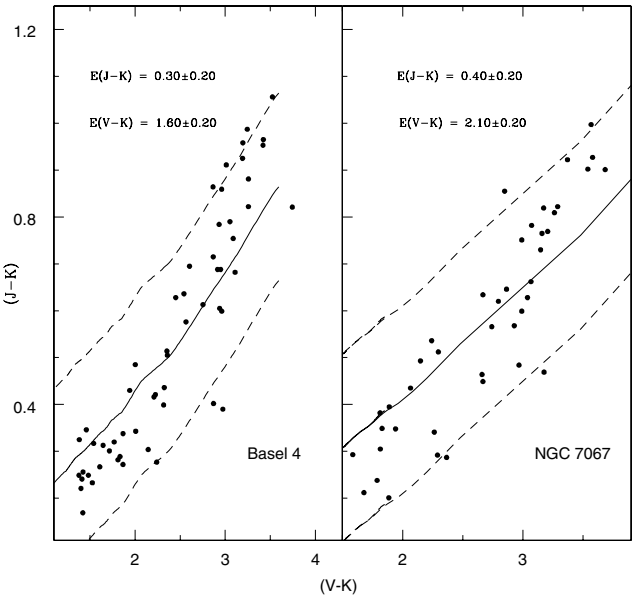

Figure 6. The $(J - K)$ versus $(V - K)$ colour–colour diagram of all the stars that are common in V and JHK data within the cluster radius for the cluster Basel 4 and NGC 7067. The solid line is a ZAMS fitted for the marked values of colour excesses. Dashed lines show the error bar.

4.3.3 Near-IR excess fluxes

An infrared excess is produced by the stars which have their own envelope of gas and dust. To investigate the near-IR flux in the stars of the clusters under study, we plotted $\Delta(V - H)$ and $\Delta(V - K)$ against $E(V - J)$ in Fig. 8. The differences between the observed colour excess in $(V - H)$ and $(V - K)$ based on spectral classification and the derived colour excess from $E(V - J)$ assuming a normal extinction law are calculated. The differences can be considered statistically significant only if their absolute values are larger than ∼0.5 mag. The short-dashed lines in Fig. 8 represent the extent of expected errors. Observational uncertainties in JHK magnitudes, inaccuracies in estimation of $E(V - J)$ and errors in spectral classification may play major role in the determination of differences. An inspection of Fig. 8 shows that the absolute values of $\Delta(V - H)$ and $\Delta(V - K)$ are close to zero for all the members. This indicates that there is no signature of near-IR excess fluxes.

4.4 Distance to the clusters

The ZAMS fitting procedure was employed to derive the distances of the clusters. Fig. 9 shows the intrinsic CM diagrams for Basel 4 and NGC 7067 which is plotted by considering the probable cluster members. For converting apparent V magnitude and $(U - B)$, $(B - V)$, $(V - R)$ and $(V - I)$ colours into intrinsic one, we used average

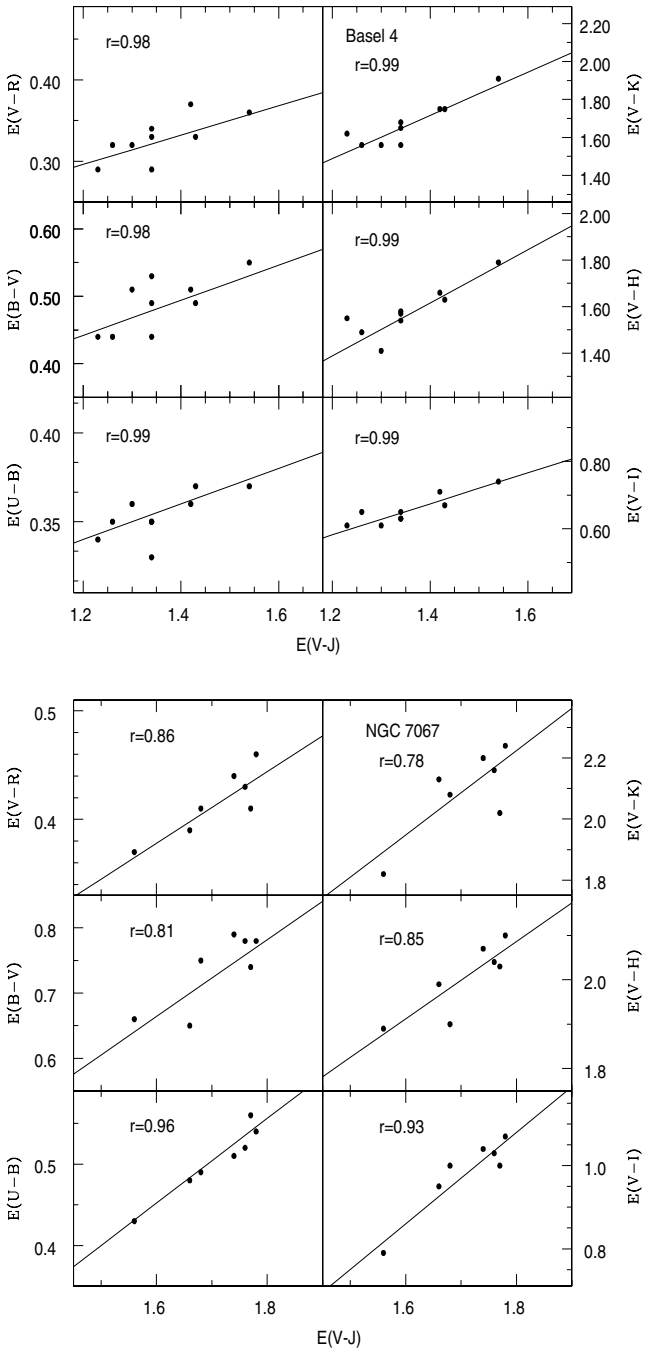

Figure 7. The plot of $E(U-B)$, $E(B-V)$, $E(V-R)$ $E(V-I)$, $E(V-H)$ and $(V-K)$ against $E(V-J)$ for Basel 4 and NGC 7067. The solid line in each diagram represents the least-squares linear fit to the data points. The values of correlation coefficients are shown in the diagram.

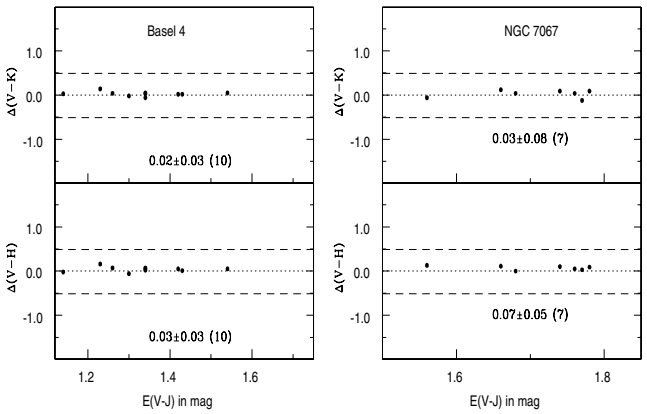

Figure 8. Plots of near-IR flux excess/deficiency in terms of $\Delta(V-H)$ and $\Delta(V-K)$ against the colour excess $E(V-J)$ for Basel 4 and NGC 7067. The horizontal dotted lines denote zero excess. The short-dashed lines denote the extent of the expected errors.

values of $E(B-V)$ and found the following relations for $E(U-B)$(cf. Kamp 1974; Sagar & Joshi 1979), A_v and $E(V-I)$ (Walker 1987) and $E(V-R)$ (Alcalá & Ferro 1988):

$$E(U-B) = [X + 0.05E(B-V)]E(B-V),$$

where $X = 0.62 - 0.3(B-V)_0$ for $(B-V)_0 < -0.09$
and $X = 0.66 + 0.08(B-V)_0$ for $(B-V)_0 > -0.09$.

$$A_v = [3.06 + 0.25(B-V)_0 + 0.05E(B-V)]E(B-V)$$

and $E(V-R) = [E1 + E2E(B-V)]E(B-V)$
where $E1 = 0.6316 + 0.0713(B-V)_0$
and $E2 = 0.0362 + 0.0078(B-V)_0$;

$$E(V-I) = 1.25[1 + 0.06(B-V)_0 + 0.014E(B-V)]E(B-V).$$

The ZAMS for $Z = 0.008$ is plotted in $V_0, (U-B)_0$; $V_0, (B-V)_0$; V_0, $(V-R)_0$ and V_0, $(V-I)_0$ diagrams of Basel 4 are taken from Schaerer et al. (1993). In V_0, $(U-B)_0$ and V_0, $(B-V)_0$ diagrams of NGC 7067, we fitted the solar metallicity ZAMS given by Schmidt-Kaler (1982) while that given by Walker (1985) was fitted in the V_0, $(V-I)_0$ diagram. For V_0, $(V-R)_0$ diagram, we have calculated $(V-R)_0$ using its relation with $(B-V)_0$ given by Caldwell et al. (1993). The good fitting of the ZAMS to the intrinsic CM diagrams was achieved for a distance modulus $(m-M)_0$ as 12.4 $\pm$ 0.2 and 12.8 $\pm$ 0.2 mag for Basel 4 and NGC 7067 respectively. The corresponding distances are 3.0 $\pm$ 0.2 and 3.6 $\pm$ 0.2 kpc. The fact that we were able to find faint probable cluster members allows us to get a better definition of the cluster lower main sequence, which in turn improves the estimation of the distances. The distance of the cluster Basel 4 is estimated as 3.0 $\pm$ 0.2 kpc, which is smaller than the value 5.6 kpc given by Svolopoulos (1965) based on RGU

Table 8. A comparison of extinction law in the direction of Basel 4 and NGC 7067 with normal extinction law given by Cardelli et al. (1989).

Objects	$\frac{E(U-B)}{E(V-J)}$	$\frac{E(B-V)}{E(V-J)}$	$\frac{E(V-R)}{E(V-J)}$	$\frac{E(V-I)}{E(V-J)}$	$\frac{E(V-H)}{E(V-J)}$	$\frac{E(V-K)}{E(V-J)}$	$\frac{E(J-K)}{E(V-K)}$
Normal value	0.32	0.43	0.27	0.56	1.13	1.21	0.19
Basel 4	0.26 $\pm$ 0.02	0.36 $\pm$ 0.02	0.25 $\pm$ 0.02	0.49 $\pm$ 0.05	1.16 $\pm$0.04	1.24 $\pm$ 0.04	0.20 $\pm$ 0.30
NGC 7067	0.30 $\pm$ 0.01	0.43 $\pm$ 0.02	0.24 $\pm$ 0.08	0.57 $\pm$ 0.03	1.17 $\pm$0.03	1.22 $\pm$ 0.05	0.20 $\pm$ 0.30

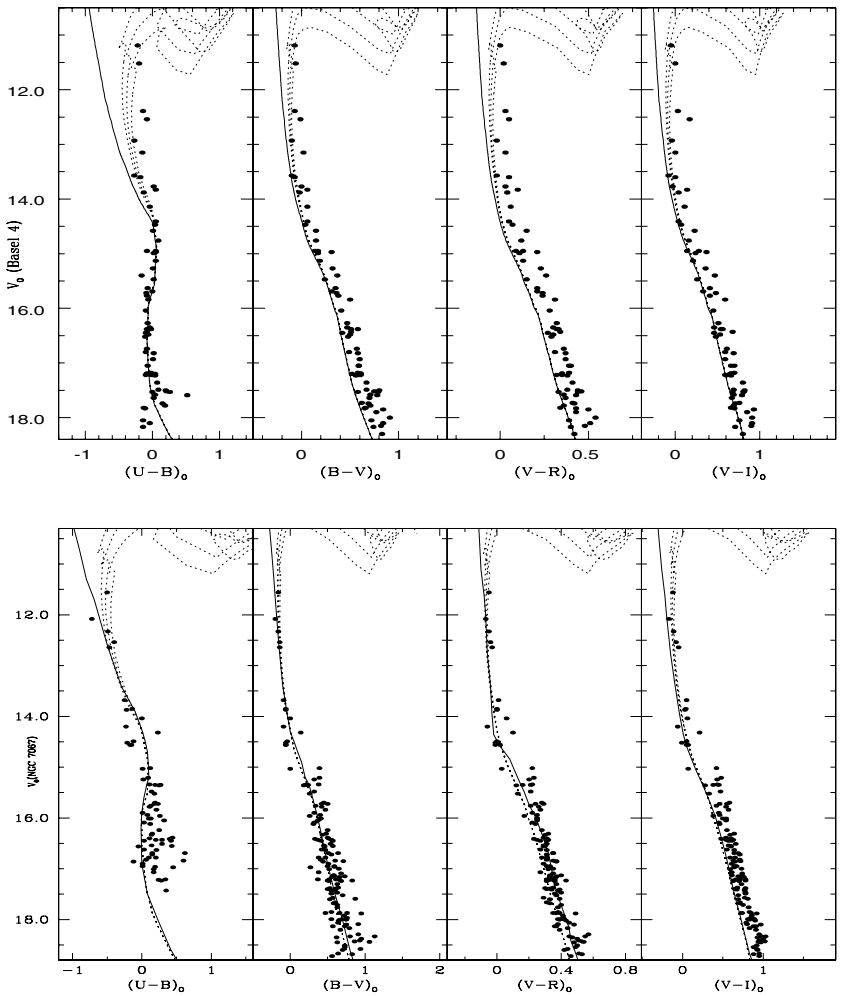

Figure 9. The $V_0, (U-B)_0$; $V_0, (B-V)_0$; $V_0, (V-R)_0$ and $V_0, (V-I)_0$ diagrams for stars of the Basel 4 and NGC 7067. The continuous curves, ZAMS fitted to the MS and dotted curves are the isochrones for $Z = 0.008$ stars of log(age) = 8.2, 8.3 and 8.4 for Basel 4 and $Z = 0.02$ stars of log(age) = 7.9, 8.0 and 8.1 for NGC 7067.

photographic photometry. We derived 3.6 ± 0.2 kpc distance for the cluster NGC 7067, which is also the value given by Lyngå (1987). The distance of this cluster is 1.3 kpc given in the catalogue of Dias et al. (2002), which is much smaller than the value estimated by us.

4.5 Ages of the clusters

The ages of the clusters are determined with the aid of the isochrones in the intrinsic CM diagrams (Fig. 9) of $Z = 0.008$ taken from Schaerer et al. (1993) for Basel 4 and $Z = 0.02$ taken from Schaller et al. (1992) for NGC 7067. The isochrones are computed by considering the mass loss and convective core overshooting. By fitting the isochrones to the cluster upper sequence of Fig. 9, we found age of 200 ± 50 and 100 ± 25 Myr for Basel 4 and NGC 7067 respectively. For the clusters Basel 4 and NGC 7067, our estimated values are larger than the values given in Lyngå (1987) and Dias et al. (2002) catalogues.

Using the optical as well as near-IR data, we redetermined the distance and age of both the clusters. Fig. 10 represents V vs $(V-K)$ and K vs $(J-K)$ CM diagrams. We have fitted the theoretical isochrones given by Schaerer et al. (1993) ($Z = 0.008$) of log(age) = 8.3 for Basel 4 and by Schaller et al. (1992) ($Z = 0.02$) of log(age) = 8.0 for NGC 7067. The apparent distance moduli $(m-M)_{V,(V-K)}$ and $(m-M)_{K,(J-K)}$ turn out to be 13.9 ± 0.3 and 12.5 ± 0.3 mag for Basel 4 and 15.0 ± 0.3 and 13.0 ± 0.3 mag for NGC 7067 respectively. By using the reddening estimated in the previous section we derive a distance of 3.1 ± 0.2 and 3.7 ± 0.2 kpc for Basel 4 and NGC 7067 respectively. Both age and distance determination for both the clusters are thus in agreement with our earlier estimates. However, the scatter is larger because of the larger errors on the *JHK* magnitudes.

4.6 Luminosity and mass function of the clusters

Since, our first aim is to derive the luminosity function from star counts then it is necessary to draw our attention on the completeness of the derived star list. Owing to the stellar crowding on the CCD frame and efficiency of the data reduction programmes, not all the stars of the frame may be detected. For deriving the completeness factor (CF) we used the V versus $(V-I)$ CM diagram instead of others because it is deepest. The detailed procedure for deriving the CF is given below.

4.6.1 Determination of photometric completeness

To know about the completeness of our photometric data, we performed experiments with artificial stars using the ADDSTAR routine

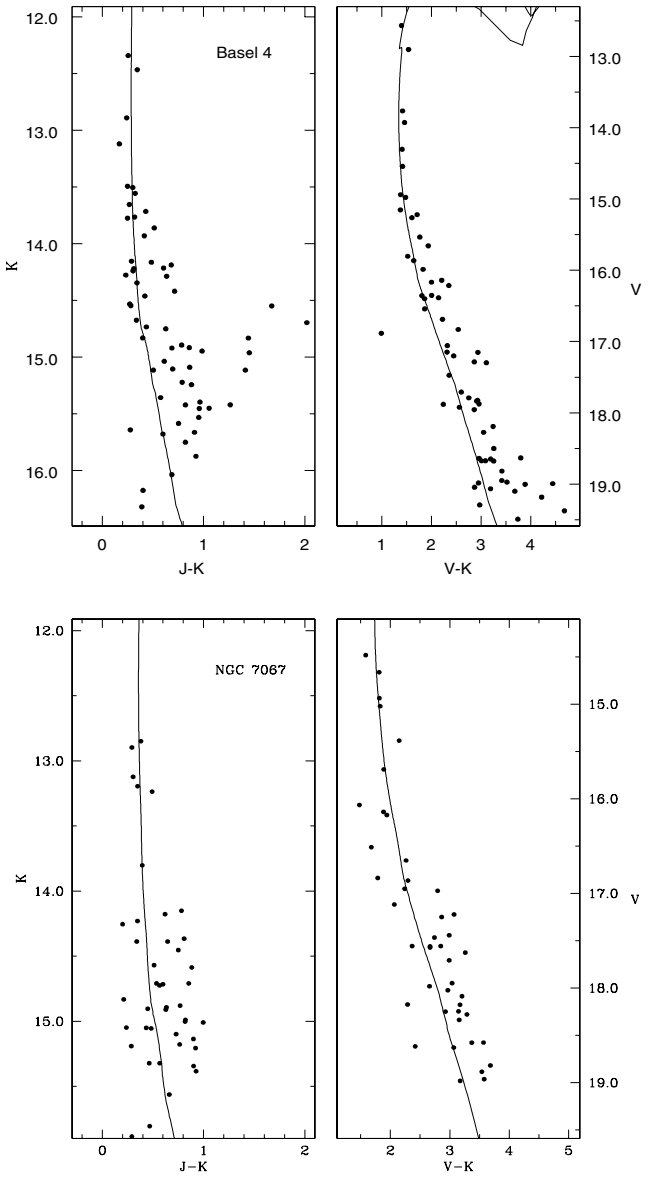

Figure 10. The K, $(J-K)$ and V, $(V-K)$ diagrams of the sample stars in the cluster Basel 4 and NGC 7067.

in DAOPHOT II. In this experiment a number of stars are added randomly in different magnitude bin to the CCD original V frame. For the I-band image the added stars have same geometrical positions but differ in I brightness according to the mean $(V-I)$ colour of the MS stars. In order to avoid overcrowding of the images by the additional stars, we added only 10 per cent of the number of stars actually detected. The luminosity distribution of the artificial stars has been chosen in such a way that more stars are inserted into the fainter magnitude bins. The photometric routines are run on these images with the same set of parameters as for the original images, and determined the number of the ad stars that are found. We estimated the CF as the ratio between the number of artificial stars recovered simultaneously in the V and I passbands and the number of added stars per one-magnitude bin. Table 9 lists the CF values for both clusters under study in the V-band image. For determining the CF, a number of methods have been described by various authors (cf. Stetson 1987; Mateo 1988; Sagar & Richtler 1991; Banks,

Table 9. Variation of completeness factor (CF) in the V, $(V-I)$ diagram with the MS brightness in both clusters.

V mag range	Basel 4	NGC 7067
13–14	0.98	0.99
14–15	0.98	0.99
15–16	0.97	0.98
16–17	0.94	0.95
17–18	0.92	0.93
18–19	0.90	0.91
19–20	0.87	0.89

Dodd & Sullivan 1995) in a CM diagram. We adopted the procedure of Sagar & Richtler (1991) as this method recovered the actual LF better with a mean error of 3 per cent up to CF > 0.5 (Mateo 1988).

4.6.2 Determination of mass function

To construct the luminosity and mass function of the clusters we need to correct the luminosity distribution of our selected sample for field star contamination. To quantify the contamination we adopted the criterion described in Section 4.2. In the V, $(V-I)$ CM diagram we defined a strip for the MS of the cluster region, and the same strip was also drawn in the CM diagram of the corresponding field region as shown in Fig. 4. Further, we determined the number of stars belonging to the strip in the cluster region as well as in the field region in each magnitude bin. In this way we can estimate the number of field stars present in various magnitude bins of the cluster region. The observed LFs of the cluster and field regions were also corrected for data incompleteness as well as for differences in area. The true LF for the cluster was obtained by subtracting the observed LF of the field region from the observed LF of the cluster region. The MF slope has been derived from the mass distribution $\xi(M)$. If dN represents the number of stars in a mass bin dM with central mass M, then the value of slope x is determined from the linear relation

$$\log \frac{\mathrm{d}N}{\mathrm{d}M} = -(1+x) \times \log(M) + \text{constant}$$

using the least-squares solution. The Salpeter (1955) value for the slope of MF is $x = 1.35$.

Theoretical models by Schaller et al. (1992) for NGC 7067 and by Schaerer et al. (1993) for Basel 4, along with the cluster parameters derived by us, have been used to convert the observed luminosity function to the mass function. The plot of MFs of Basel 4 and NGC 7067 is shown in Fig. 11. The value of the MF slope along with the mass range and error are given in Table 10, where the quoted errors are derived from the linear least-squares fit to the data points. Our estimated value of MF slope x is in agreement with the Salpeter (1955) value within the error for both the clusters. However, the error in MF slope is large owing to poor statistics of cluster members.

4.7 Mass segregation

In order to investigate the cluster dynamical evolution and mass segregation effect owing to energy equipartition, we subdivided the stars into three mass ranges: $3.5 \leqslant \mathrm{M}_{\odot} < 2.0$, $2.0 \leqslant \mathrm{M}_{\odot} < 1.0$ and $\mathrm{M}_{\odot} < 1.0$ for Basel 4 and $4.5 \leqslant \mathrm{M}_{\odot} < 2.5$, $2.5 \leqslant \mathrm{M}_{\odot} < 1.0$ and $\mathrm{M}_{\odot} < 1.0$ for NGC 7067. In Fig. 12 we present cumulative radial stellar distribution of stars for different masses. An inspection of

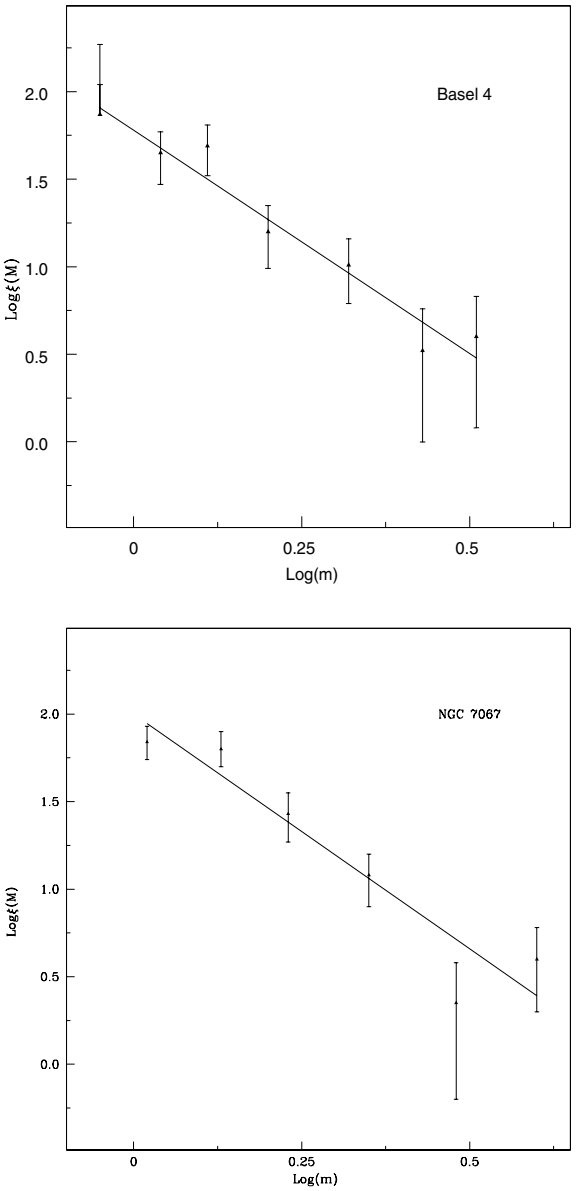

Figure 11. The plot shows the mass functions derived using theoretical models of Schaerer et al. (1993) for Basel 4 and of Schaller et al. (1992) for NGC 7067.

Table 10. The slope of the mass function derived from the LF along with relaxation time T_E.

cluster	Mass range $M_\odot$	Mass Function slope (x)	log T_E
Basel 4	0.8–3.5	1.55 ± 0.25	7.0
NGC 7067	0.9–4.5	1.68 ± 0.47	7.1

Fig. 12 shows that both the clusters show a mass segregation effect. To check whether these mass distributions represent the same kind of distribution or not we perform the Kolmogorov–Smirnov (K–S) test. This test shows that mass segregation has taken place at a confidence level of 65 per cent for Basel 4 and 70 per cent for NGC 7067. Further, it is important to know whether existing mass

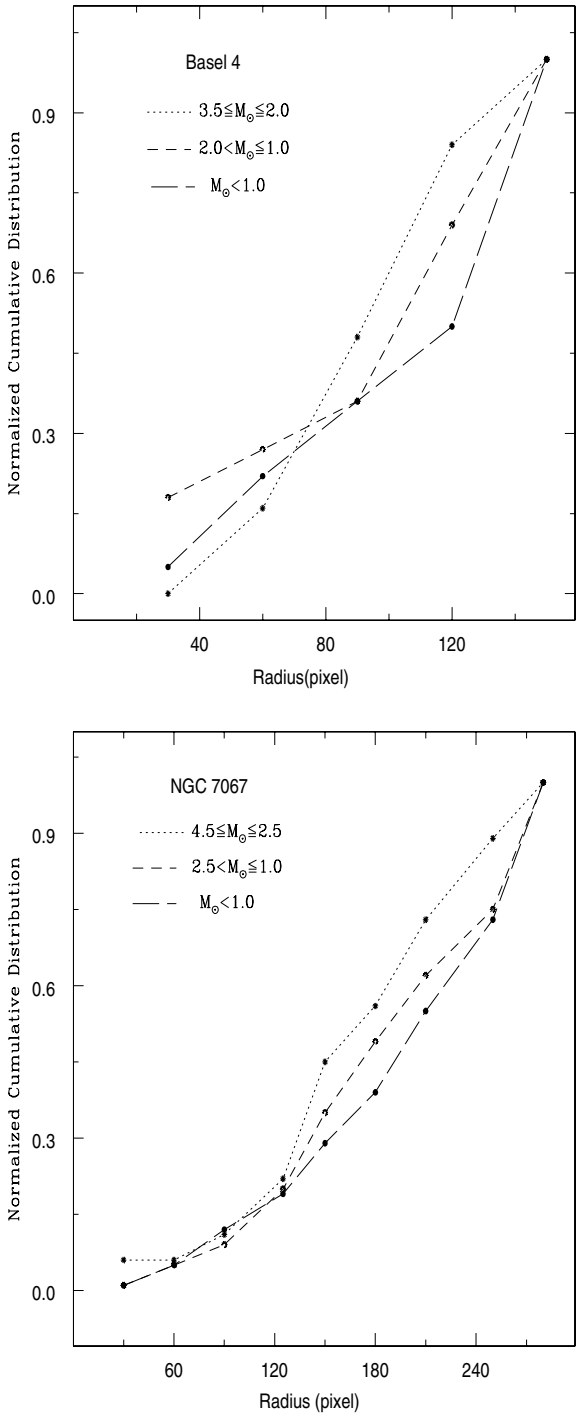

Figure 12. Cumulative radial distribution of stars in different mass ranges for Basel 4 and NGC 7067.

segregation is caused by dynamical evolution or the imprint of the star formation process.

One of the possible causes of mass segregation is the dynamical evolution of clusters. Over the lifetime of a star cluster, encounters between its member stars gradually lead to an increased degree of energy equipartition throughout the cluster. The most important result of this process is that the higher-mass cluster members gradually sink towards the cluster centre and in the process transfer their kinetic energy to the more numerous lower-mass stellar component,

thus leading to mass segregation. The time-scale on which a cluster will have lost all traces of its initial conditions is well represented by its relaxation time T_E. It is given by

$$T_E = \frac{8.9 \times 10^5 N^{1/2} R_h^{3/2}}{\langle m \rangle^{1/2} \log(0.4N)},$$

where N is the number of cluster members, R_h is the radius containing half of the cluster mass and $\langle m \rangle$ is the mean mass of the cluster stars (cf. Spitzer & Hart 1971). The number of probable MS stars is estimated using the CM diagrams of the clusters after subtracting the contribution from field stars and applying the necessary corrections for the data incompleteness. For determining the R_h, we assume that the R_h is equal to half of the cluster radius estimated by us. The angular values are converted to linear values using the cluster distances which are derived here. Inclusion of cluster members fainter than the limiting V magnitude will decrease the value of $\langle m \rangle$ and increase the value of N. This will result in higher values of T_E. Hence the T_E values obtained here may be considered as the lower limit.

A comparison of cluster age with its relaxation time indicates that the relaxation time is smaller than the age of the clusters. Thus we can conclude that the clusters under study are dynamically relaxed. It may be the result of dynamical evolution or the imprint of star formation processes or both.

5 CONCLUSIONS

In this paper we have presented CCD *UBVRI* photometry for the stars in the fields of open clusters Basel 4 and NGC 7067 for the first time. Using present CCD data in combination with 2MASS data we derive the following results.

(i) Using the $(U - B)$ versus $(B - V)$ colour–colour diagram, we determine the cluster metallicity $Z \sim 0.008$ and 0.02 for Basel 4 and NGC 7067 respectively. The corresponding mean value of $E(B - V) = 0.45 \pm 0.05$ mag and 0.75 ± 0.05 mag respectively. Interstellar extinction law has also been studied, using optical as well as near-IR data, and we found that it is normal in the direction of both the clusters. The colour–colour diagram gives the colour excess $E(J - K) = 0.30 \pm 0.20$ mag and $E(V - K) = 1.60 \pm 0.20$ mag for Basel 4 and $E(J - K) = 0.40 \pm 0.20$ mag and $E(V - K) = 2.10 \pm 0.20$ mag for NGC 7067.

(ii) Basel 4 and NGC 7067 are located at a distance of 3.0 ± 0.2 and 3.6 ± 0.2 kpc respectively. The corresponding ages are 200 ± 50 and 100 ± 25 Myr respectively. They are determined by fitting the isochrones of Schaerer et al. (1993) for $Z = 0.008$ in Basel 4 and of Schaller et al. (1992) for $Z = 0.02$ in NGC 7067. Using the 2MASS data we also derived the distance and age of both the clusters, and they are in agreement with those derived using optical data.

(iii) The radial density profiles show that the radius of Basel 4 and NGC 7067 are 1.8 and 3.0 arcmin respectively, which indicate that the clusters under study are compact. At the cluster distance, they correspond to linear radius of $\sim$1.6 and 3.2 pc respectively.

(iv) The values of MF slope are 1.55 ± 0.25 and 1.68 ± 0.47 for Basel 4 and NGC 7067 respectively. They are determined by applying the corrections of data incompleteness and field star contamination and are in agreement with the Salpeter (1955) value.

(v) Mass segregation is observed in both Basel 4 and NGC 7067 in the sense that massive stars tend to lie near the cluster centre. The dynamical relaxation time indicates that both the clusters are dynamically relaxed. Thus mass segregation might have occurred owing to dynamical evolution, the imprint of star formation or both.

ACKNOWLEDGMENTS

We thank the referee for valuable comments, which have improved the quality of this paper. We are grateful to Dr Vijay Mohan for helping in data reduction. This study made use of 2MASS and WEBDA.

REFERENCES

Alcalá J. M., Ferro A. A., 1988, Rev. Mex. Astron. Astrofis., 16, 81
Banks T., Dodd R. J., Sullivan D. J., 1995, MNRAS, 274, 1225
Becker W., 1963, Z. Astrophys., 57, 117
Becker W., 1965, Mem. Soc. Astron. Ital., 36, 283
Caldwell A. R. John, Cousins A. W. J., Ahlers C. C., Wamelen P. van, Maritz E. J., 1993, SAAO Circ. 15
Cardelli J. A., Clayton G. C., Mathis J. S., 1989, ApJ, 345, 245
Carney B. W., 1979, ApJ, 233, 211
Dias W. S., Alessi B. S., Moitinho A., Lépine J. R. D., 2002, A&A, 389, 871
FitzGerald M. P., 1970, A&A, 4, 234
Hassan S. M., 1973, A&AS, 9, 261
Johnson H. L., 1966, ARA&A, 4, 193
Johnson H. L., Morgan W. W., 1953, ApJ, 117, 313
Johnson H. L., 1968, in Middlehurst B. M., Aller L. H., eds, Nebullae and Interstellar Matter. Univ. Chicago Press, Chicago, 191
Kaluzny J., 1992, Acta Astron., 42, 29
Kamp L. W., 1974, A&AS, 16, 1
Koornneef J., 1983, A&A, 128, 84
Landolt A. U., 1992, AJ, 104, 340
Lyngå G., 1987, in Catalog of open cluster data, Computer Based Catalogue available through the CDS, Strasbourg, France and through NASA Data Centre GreenBelt, MaryLand, USA, 5th edition, vol. 4, p. 121 (http://cdsweb.u-strasbg.fr)
Mateo M., 1988, ApJ, 331, 261
Mermilliod J. C., 1995, in Egret E., Albrecht M. A., eds, Information and on-line data in Astronomy. Kluwer Academic PressM, Dordrecht, p. 227
Persson S. E., Murphy D. C., Krzeminski W., Roth M., Rieke M. J., 1998, AJ, 116, 2475
Sagar R., Joshi U. C., 1979, Ap&SS, 66, 3
Sagar R., Richtler T., 1991, A&A, 250, 324
Salpeter E. E., 1955, ApJ, 121, 161
Schaerer D., Meynet G., Maeder A., Schaller G., 1993, A&AS, 98, 523
Schaller G., Schaerer D., Meynet G., Maeder A., 1992, A&AS, 96, 269
Schmidt-Kaler Th., 1982, in Scaifers K., Voigt H. H., eds, Landolt/Bornstein, Numerical Data and Functional Relationship in Science and Technology, New series, Group VI, Vol. 2b. Springer-Verlag, Berlin, p. 14
Spitzer L., Hart M. H., 1971, ApJ, 164, 399
Stetson P. B., 1987, PASP, 99, 191
Svolopoulos S. N., 1965, Z. Astrophys., 61, 97
Walker A. R., 1985, MNRAS, 213, 889
Walker A. R., 1987, MNRAS, 229, 31
Whittet D. C. B., van Breda I. G., 1980, MNRAS, 192, 467
Yadav R. K. S., Sagar R., 2002, MNRAS, 337, 133

This paper has been typeset from a TEX/LATEX file prepared by the author.